Materials Transactions, Vol. 64, No. 9 (2023) pp. 2124 to 2127
Special Issue on Nanostructured Functional Materials and Their Applications IV

Fundamentally Different Magnetoresistance Mechanisms in Related Co/Pd and Co/Pt Multilayers for Spintronic Applications

W.-B. Wu[1], J. Kasiuk[2], J. Przewoźnik[3], Cz. Kapusta[3], I. Svito[2], K. Tung Do[4], T. Huong Nguyen[4], H. Manh Dinh[5], J. Åkerman[6] and T.N. Anh Nguyen[4,7,*]

[1]*College of Physical Science and Technology, Dalian University, Dalian, 116622, China*
[2]*Belarusian State University, Minsk, 220030, Belarus*
[3]*AGH University of Krakow, Faculty of Physics and Applied Computer Science, Department of Solid State Physics, Krakow, 30-059, Poland*
[4]*Institute of Materials Science, Vietnam Academy of Science and Technology, 18 Hoang Quoc Viet, Cau Giay, Hanoi 11355, Vietnam*
[5]*Physics Department, Hanoi National University of Education, 144 Xuan Thuy, Hanoi, Vietnam*
[6]*Department of Physics, University of Gothenburg, Göteborg 41296, Sweden*
[7]*Graduate University of Science and Technology, Vietnam Academy of Science and Technology, 18 Hoang Quoc Viet, Cau Giay, Hanoi 11355, Vietnam*

In this research, we have analyzed the electrical resistance of Co/Pd and Co/Pt thin multilayered films with perpendicular magnetic anisotropy (PMA) deposited by magnetron sputtering to determine and compare their magnetoresistance (MR) mechanisms. The studies were carried out depending on the magnitude and direction of the applied magnetic field in a wide temperature range $T = 3$–300 K. It is shown that both the isotropic and angle-dependent MR mechanisms are different for these two films studied. Magnon and anisotropic MR mechanisms (MMR and AMR) are found to be characteristic of the Co/Pd film, while Lorentz and spin Hall MR mechanisms (LMR and SMR) determine the magnetotransport in the Co/Pt film. The revealed differences in the MR mechanisms are discussed in terms of the quality of interfaces and properties of *5d* (*4d*) metals. [doi:10.2320/matertrans.MT-MG2022018]

(Received January 12, 2023; Accepted May 22, 2023; Published August 25, 2023)

Keywords: *multilayered films, perpendicular magnetic anisotropy, anisotropic magnetoresistance, magnons, spin Hall effect*

1. Introduction

The mechanisms of electron and spin transport in *3d ferromagnet* (FM)/*5d(4d) heavy metal* (HM) bilayers and multilayers (MLs) are of great interest for spintronics due to their high potential for magnetic memory applications.[1,2)] Among them, $[Co/Pt]_n$ and $[Co/Pd]_n$ MLs have a strong and tunable perpendicular magnetic anisotropy (PMA).[3–9)] Both Pt and Pd are paramagnetic transition metals of group 10 (same group as Ni), which can be polarized in the vicinity of a FM layer and carry magnetic moments.[10)] The hybridization between *3d* electron orbitals of Co and *5d*(*4d*) orbitals of Pt(Pd) at the FM/HM interfaces and spin-orbit coupling (SOC), induced by symmetry breaking, are responsible for the strong interfacial magnetic anisotropy, which mainly contributes to PMA of $[Co/Pt]_n$ and $[Co/Pd]_n$ MLs.[7,11–13)] The strong PMA makes these MLs suitable for high density data storage, while the essential SOC in the *5d* (Pt, Ta, W, Hf) and *4d* (Pd) HM enables a field-free magnetization switching of the FM layer (Co,[3,14)] NiCo,[2)] CoFe(B)[1,13)]), which underlies new magnetic recording technologies.[1–3,13–17)] In such FM/HM bilayers, a spin accumulation at the interface via the mechanisms known as spin Hall effect (SHE) and Rashba-Edelstetin effect can exert a torque on the magnetic moments of the FM layer leading to their precession or even complete reversal.[1,13–17)] Therefore, the search for novel materials with a strong SOC and design of multilayered compositions by combining the layers and interfaces for enhancing the efficiency of magnetization switching are of undoubtful importance.

*Corresponding author, E-mail: ngocanhnt.vn@gmail.com

Although the Co/Pt and Co/Pd bilayers are the basic systems for designing spintronic materials, and have been studied for decades,[1–10,16,17)] there are still unclear issues related to their magnetotransport. Despite the similarity of electronic structure and magnetic properties, they demonstrate completely different magnetoresistance (MR) mechanisms, which are reported in this work. The revealed discrepancies are discussed in terms of effects associated with the band structure and interface state, since differences in SOC and induced magnetism of HM,[3)] as well as in smoothness and integrity of interfaces[5,18)] can be responsible.

2. Experimental Procedure

The thin films of $[Co/Pd]_5$ and $[Co/Pt]_5$ MLs were deposited on flat Si/SiO_2 wafers using ultra-high vacuum magnetron sputtering (*AJA International, Inc.*) at room temperature (RT). The nominal compositions of the films are the following:

$Ta_{5\,nm}/Pd_{15\,nm}/[Co_{0.5\,nm}/Pd_{1\,nm}]_{x5}/Co_{0.5\,nm}/Pd_{3\,nm}/Ta_{5\,nm}$;

$Ta_{5\,nm}/Pt_{15\,nm}/[Co_{0.4\,nm}/Pt_{0.8\,nm}]_{x5}/Co_{0.4\,nm}/Pt_{3\,nm}/Ta_{5\,nm}$ for the films marked hereafter as Co/Pd and Co/Pt MLs, respectively. The top $Pd(Pt)_{3\,nm}/Ta_{5\,nm}$ bilayer was used to prevent oxidation of the MLs, while the bottom $Ta_{5\,nm}/Pd(Pt)_{15\,nm}$ bilayer served to promote (111) texture and improve the PMA of the subsequent MLs.

Microstructural studies have been performed with a high resolution transmission electron microscopy (HRTEM) technique using an FEI Tecnai G2 F20 X-Twin microscope (200 kV). The HRTEM data were analyzed with Gatan DM software.

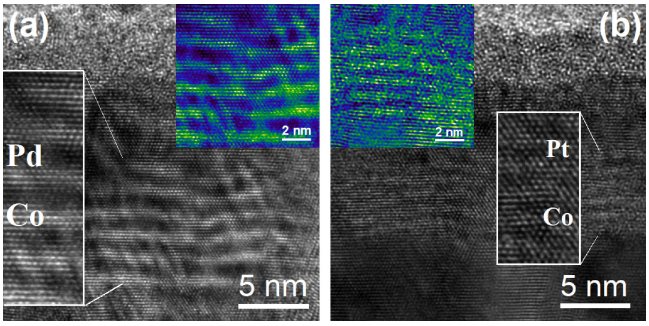

Fig. 1 Cross-sectional HRTEM images of $[Co/Pd]_5$ (a) and $[Co/Pt]_5$ (b) MLs. The insets show enlarging and coloring of the corresponding images (blue for Pd(Pt) and green for Co) for better visualization of interfaces and mixing of elements.

Measurements of the field and angular dependences of electrical resistance $R(B)$ and $R(\theta_B)$ were carried out with the four-probe method using the resistivity option of a *Quantum Design* Physical Property Measurement System (PPMS) at $T = 3$–300 K. A magnetic field with induction B up to 9 T was applied along the film normal (z direction) and in the film plane along y direction, or rotated in the zy plane which is perpendicular to charge current I (x direction).

3. Results and Discussions

The cross-sectional images of the studied Co/Pd and Co/Pt MLs, obtained by HRTEM technique, are shown in Fig. 1.

The films demonstrate a distinct layered structure. The layers of Co (lighter color) and HM (darker color) are clearly distinguishable both within the $[Co/Pd]_5$ (Fig. 1(a)) and $[Co/Pt]_5$ (Fig. 1(b)) MLs that excludes homogeneous atoms mixing and alloying the Co and Pd(Pt) layers. The atoms are arranged in a face-centered cubic (fcc) lattice within both MLs, with a preferential orientation of the (111) plane parallel to the film surface being detected. The latter is consistent with the fcc (111) texture of the studied films revealed by X-ray diffraction.[6] The interplanar distance $d_{(111)}$ estimated from HRTEM images is almost unchanged with depth within the MLs and averages 2.213 Å for Co/Pt and 2.207 Å for Co/Pd MLs. Despite the general similarity, a more pronounced interfacial mixing of atoms from neighboring layers can be revealed for the Co/Pt MLs (inset to Fig. 1(b)). Inversely, laterally consistent and more abrupt interfaces are typical of the Co/Pd MLs (Fig. 1(a)).[18] Since the deposition conditions were kept the same for both MLs, the observed differences can attribute to the material-related factors.[7] The differences in surface energy and lattice constants between the FM and HM layers are supposedly important for the processes of atoms intermixing and interfacial inter-diffusion.

Angular dependences of electrical resistance $R(\theta_B)$ on the out-of-plane orientation θ_B of the magnetic field B with respect to the film normal ($\theta_B = 0$) are shown in Fig. 2 for the Co/Pd and Co/Pt MLs. The shape of $R(\theta_B)$ curves of Co/Pd MLs doesn't depend on temperature and is characterized by two clear minima at $\theta_B = 90°$ and 270° (Fig. 2(a)). It can be approximated by the expression $R(\theta_B) = R_0 - \Delta R \cdot \sin^2\theta$,

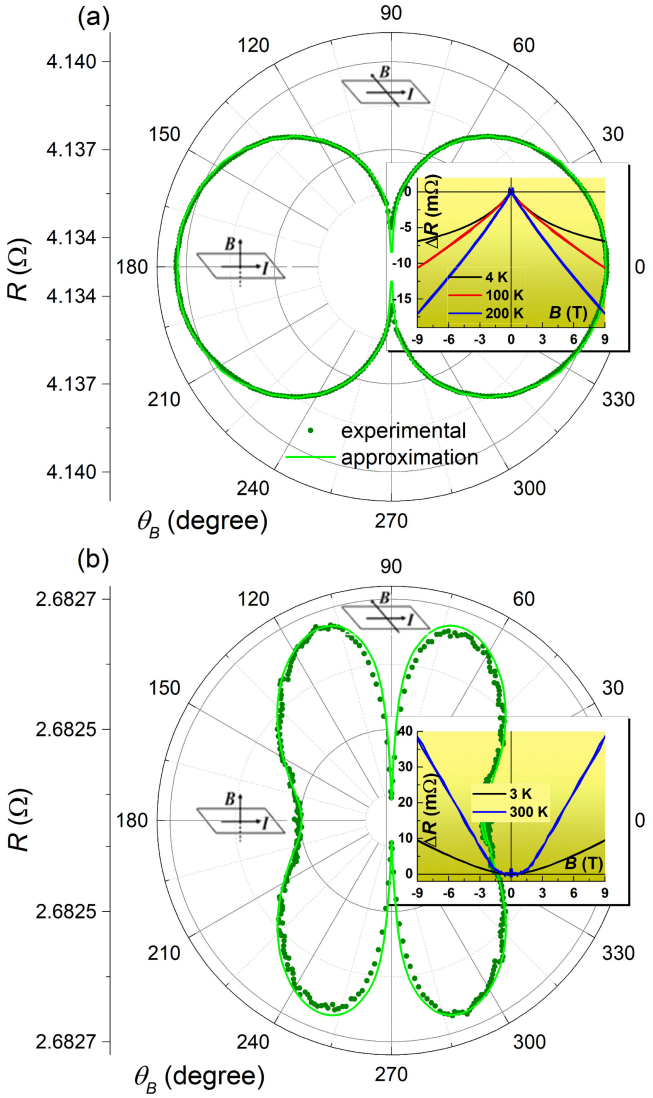

Fig. 2 Angular dependences of electrical resistance $R(\theta_B)$ of the Co/Pd (a) and Co/Pt (b) MLs measured in the external field B of 2 T at $T = 10$ K. Insets show the corresponding field dependences of resistance measured along the film normal at different temperatures.

where R_0 is the isotropic contribution to the longitudinal resistance at a certain temperature, ΔR is the amplitude of the effect, which provides angle-dependent changes in R, and θ is the polar angle, which determines the orientation of the film magnetization M with respect to the film normal ($\theta = 0$). A good correspondence of the approximation to the experimental data shown in Fig. 2(a) indicates the only angle-dependent MR mechanism for the Co/Pd film.

The shape of low-temperature $R(\theta_B)$ curves of the Co/Pt MLs, shown in Fig. 2(b), is more complex, with two additional local minima being pronounced at $\theta_B = 0$ and 180°. The latter indicates at least two contributions to the angle-dependent MR mechanism. The approximation shown in Fig. 2(b) corresponds to the relation $R(\theta_B) = R_0 - \Delta R^{(2)} \cdot \sin^2\theta - \Delta R^{(4)} \cdot \cos^4\theta$, where the $\Delta R^{(2)}$ and $\Delta R^{(4)}$ coefficients are the amplitudes of these contributions. It should be mentioned, that the local minima become less evident and gradually disappear with increasing temperature, while the shape of $R(\theta_B)$ curve becomes similar to that shown in Fig. 2(a) at RT.

Besides the different angular dependences, the Co/Pd and Co/Pt MLs demonstrate completely different field dependences of electrical resistance. The corresponding $\Delta R(B) = R(B) - R_0$ curves are illustrated in the insets to Fig. 2 for different temperatures. It is clear, that the MR effects of different signs are characteristic of these films, namely a negative MR effect is dominating for the Co/Pd MLs, while the positive MR effect is typical of the Co/Pt MLs over the whole temperature range studied. The negative MR effect in the Co/Pd MLs is identified to be realized via the magnon MR (MMR) mechanism.[9,19–21] The positive MR effect in the Co/Pt MLs relates to the Lorentz MR (LMR) mechanism,[22,23] with the magnitude of the effect being atypically increased at RT. Both mechanisms are isotropic for the field rotation in zy plane.

Pairs of $\Delta R(B)$ curves measured in two orthogonal field directions, i.e. along z and y axes, at RT are shown in Fig. 3 for both Co/Pd and Co/Pt films. In addition to the isotropic MMR and LMR effects, another negative MR mechanism is revealed, which corresponds to a decrease in R in an increasing B_y field ($\theta_B = 90°$). It is associated with the out-of-plane magnetization rotation and its tilting in the y direction at $B \leq B_A$ (B_A is the anisotropy field). The mechanism providing such an increase in R is the same as that providing the angular dependences $R(\theta_B) \sim \sin^2\theta$ shown in Fig. 2. High values of B_A field of ~3 T for the Co/Pd MLs and ~2 T for the Co/Pt MLs can be estimated from the inflection points of $\Delta R(B_y)$ curves shown in Fig. 3.

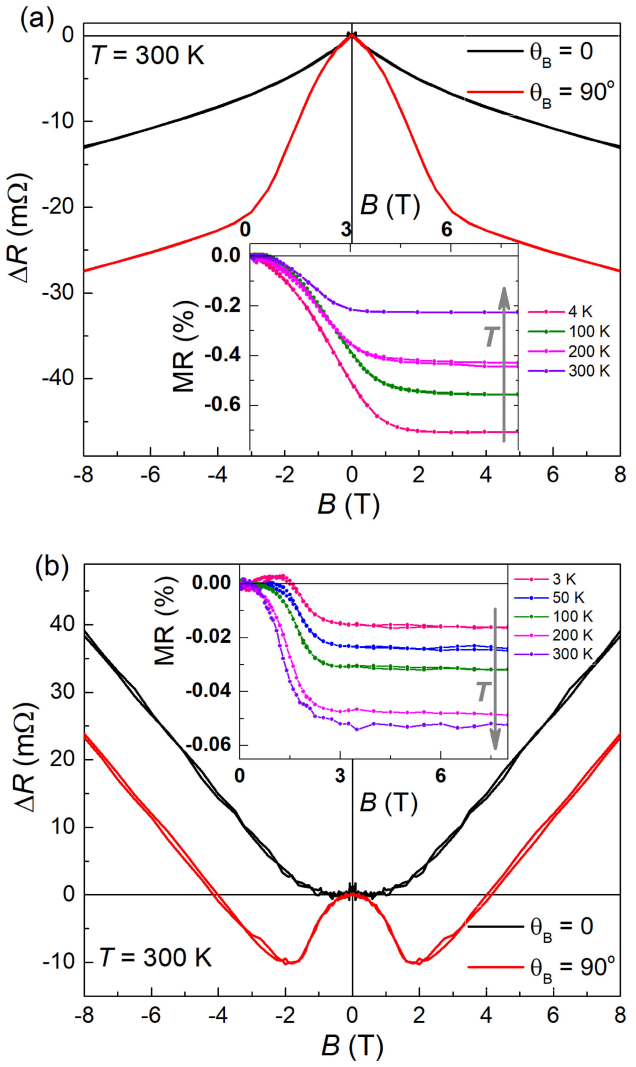

Fig. 3 Field dependences of electrical resistance $\Delta R(B)$ of the Co/Pd (a) and Co/Pt (b) MLs measured at $T = 300$ K in the external field sweeping along z ($\theta_B = 0$) and y ($\theta_B = 90°$) directions. Insets show the corresponding field dependences of angle-dependent MR effect estimated as $\mathrm{MR}(B) = 100\% \cdot (R(B_y) - R(B_z))/R(B = 0)$.

The difference between the resistance in a magnetic field oriented along $\theta_B = 90°$ and $\theta_B = 0$ directions, i.e. $R(B_y) - R(B_z)$, represents the angle-dependent contribution to the MR effect. The field dependences of this parameter, reduced to the zero-field R_0 value, are shown in the insets to Fig. 3 for the Co/Pd and Co/Pt MLs. The analysis reveals the peculiarities of angle-dependent MR effect, which is characteristic of each of the studied films. For example, the magnitude of the effect increases with decreasing temperature for the Co/Pd MLs and, inversely, decreases for the Co/Pt MLs, indicating its different nature for these two films. In addition, the MR(B) dependences are non-monotonous for the Co/Pt MLs at $T < 100$ K, with a local minimum observed in the vicinity of $B = 0$ (inset to Fig. 3(b)). The latter correlates with the local minima at $\theta_B = 0$ and 180° on the $R(\theta_B)$ curves of this film (Fig. 2(b)). Another observed peculiarity of angular MR effect should be pointed out, which also distinguishes both films studied. It lies in a significant difference in the MR ratios for the films by an order of magnitude (insets to Fig. 3).

The described peculiarities of the angular MR effect, although apparently similar for both films in its $\sin^2\theta$-type dependence, however, allow it to be attributed to completely different MR mechanisms, namely anisotropic interfacial MR (AIMR)[9,24,25] and spin Hall MR (SMR)[1,15,16,22] for the Co/Pd and Co/Pt MLs, respectively. The origin of such a difference between the MR mechanisms of the films is supposed to lie mainly in their interface structure. As it is determined by HRTEM method (Fig. 1), Co atoms are mixed to different degree with different HM atoms at the interfaces, namely, a more pronounced layered structure is typical of the Co/Pd MLs (Fig. 1(a)),[8] while a more prominent local interpenetration of the layers is characteristic of the Co/Pt MLs (Fig. 1(b)).[18] Laterally consistent Co/Pd interfaces promote strong interfacial contribution to the magnetotransport of Co/Pd MLs via the AIMR mechanism. On the other hand, a significantly higher SHE in Pt compared to Pd due to its stronger SOC[7,17] ensures the manifestation of the SMR mechanism in the Co/Pt MLs. A decrease in the MR effect of Co/Pt MLs with decreasing temperature (inset to Fig. 3(b)) correlates with the tendency characteristic of the SMR mechanism, since the strong Pt polarization suppresses the effect at low temperature.[26] The obtained effects up to 0.06% are consistent with the values of the SMR effect observed for similar films (0.05% for $Pt_{4\,nm}$,[22] 0.15%[15] and 0.25%[1] for $Pt_{3\,nm}$, 0.10% for $Ta_{5\,nm}$,[1] etc.).

Besides the second-order contribution $\Delta R^{(2)} \cdot \sin^2\theta$ to the angular MR, the higher order contribution, namely fourth-order term $\Delta R^{(4)} \cdot \cos^4\theta$, is detected for the Co/Pt MLs. Its contribution is found to increase with decreasing temperature (inset to Fig. 3(b)), similarly to the AIMR effect of the Co/Pd MLs (Fig. 3(a)). This higher-order term is usually attributed

to the texture-induced contribution to the anisotropic MR (AMR),[25,27] which appears even when the magnetization rotates perpendicularly to the current. A pronounced *fcc* (111) texture is characteristic of both Co/Pd and Co/Pt MLs,[6] but due to the low magnitude of the effect (only 0.05% even at $T = 10$ K) it cannot be distinguished in the MR signal of the Co/Pd MLs because of much higher AIMR effect (~0.7% at $T = 4$–10 K). A small texture-induced AMR effect is associated with thin Co layers in the studied films. Indeed, higher values are typically obtained for significantly thicker FM layers (0.07% for $Co_{35\,nm}$ in Pt/Co/Pt; 0.6% for $Ni_{10\,nm}$ in Pt/Ni/Pt;[25] 0.8% for $CoNi_{8\,nm}$ in Pt/[Co/Ni] stacks[27]). The observation of the higher-order contributions to AMR for the studied Co/Pt MLs with such a small thickness of the FM layer is supposed to become possible due to their significantly higher PMA of ~2 T, achieved by a multiple repetition of Co/Pt bilayers, as compared to the commonly studied FM/HM bilayers.[1,17,27]

4. Conclusion

In this study, we demonstrated that apparently identical Co/Pd and Co/Pt MLs possessing high PMA of up to 3 T show completely different MR effects with different underlying mechanisms. A distinct layered structure with a Co thickness of only a few atomic monolayers and a pronounced *fcc* (111) texture typical of both of the films studied, which provide their high PMA, were found to be not sufficient criteria for obtaining reproducible effects in spin-dependent electron transport. It is shown that both the isotropic and angle-dependent MR mechanisms are different for the Co/Pd and Co/Pt MLs. The isotropic effect of magnon MR related to the FM layer dominates in the Co/Pd MLs, suppressing the conventional Lorentz MR effect, while it almost completely degenerates in the Co/Pt MLs. The angle-dependent out-of-plane MR effect in the Co/Pd MLs corresponds to an interfacial-type AIMR mechanism, while in the Co/Pt MLs it is presumably provided mainly by a bulk-type SMR mechanism originating from the Pt layer adjacent to the MLs. In addition, the texture-induced higher-order AMR term contributes to the angular MR of the Co/Pt MLs. The above differences in the MR mechanisms relate mainly to different degrees of interface integrity in the Co/Pd and Co/Pt MLs. Additionally, various intrinsic properties of *5d* Pt and *4d* Pd metals, including quantitative differences in the SHE and induced magnetism, also contribute to the revealed diversity of the MR mechanisms.

Acknowledgments

This work was financially supported by Vietnam Academy of Science and Technology under Project QTBY01.02/23-24 and Belarusian Republican Foundation for Fundamental Research (project no. F23V-003).

REFERENCES

1) Y.C. Lau and M. Hayashi: Jpn. J. Appl. Phys. **56** (2017) 0802B5.
2) C. Engel, S. Goolaup, F. Luo, W. Gan and W.S. Lew: J. Appl. Phys. **121** (2017) 143902.
3) H. Nemoto and Y. Hosoe: J. Appl. Phys. **97** (2005) 10J109.
4) C.-J. Lin, G.L. Gorman, C.H. Lee, R.F.C. Farrow, E.E. Marinero, H.V. Do, H. Notarys and C.J. Chien: J. Magn. Magn. Mater. **93** (1991) 194–206.
5) N. Figueiredo-Prestes, J. Zarpellon, D.S. Costa, I. Mazzaro, P.C. Camargo, A.J.A. Oliveira, C. Deranlot, J.M. George and D.H. Mosca: J. Phys. Chem. C **125** (2021) 4885–4892.
6) T.N. Anh Nguyen, J. Fedotova, J. Kasiuk, V. Bayev, O. Kupreeva, S. Lazarouk, D.H. Manh, D.L. Vu, S. Chung, J. Åkerman, V. Altynov and A. Maximenko: Appl. Surf. Sci. **427** (2018) 649–655.
7) N. Nakajima, T. Koide, T. Shidara, H. Miyauchi, H. Fukutani, A. Fujimori, K. Iio, T. Katayama, M. Nývlt and Y. Suzuki: Phys. Rev. Lett. **81** (1998) 5229–5232.
8) J.M. Shaw, H.T. Nembach, T.J. Silva, S.E. Russek, R. Geiss, C. Jones, N. Clark, T. Leo and D.J. Smith: Phys. Rev. B **80** (2009) 184419.
9) Y. Kachlon, N. Kurzweil and A. Sharoni: J. Appl. Phys. **115** (2014) 173911.
10) J.W. Knepper and F.Y. Yang: Phys. Rev. B **71** (2005) 224403.
11) H.K. Tan, R.J.J. Lim, H.L. Seng, J. Shanmugam, H.Y.Y. Ko, X.M. Cheng, V. Putra, Z.X. Xing, A. Soumyanarayanan and P. Ho: J. Phys. D **54** (2021) 354003.
12) T. Kubota, T. Kamada, J. Kim, A. Tsukamoto, S. Takahashi, Y. Sonobe and K. Takanashi: Mater. Trans. **57** (2016) 773–776.
13) J.C. Leutenantsmeyer, V. Zbarsky, M. von der Ehe, S. Wittrock, P. Peretzki, H. Schuhmann, A. Thomas, K. Rott, G. Reiss, T.H. Kim, M. Seibt and M. Münzenberg: Mater. Trans. **56** (2015) 1323–1326.
14) K.F. Huang, D.-S. Wang, H.H. Lin and C.H. Lai: Appl. Phys. Lett. **107** (2015) 232407.
15) Y.C. Lau, D. Betto, K. Rode, J.M.D. Coey and P. Stamenov: Nat. Nanotechnol. **11** (2016) 758–762.
16) C.O. Avci, G.S.D. Beach and P. Gambardella: Phys. Rev. B **100** (2019) 235454.
17) A. Ghosh, K. Garello, C.O. Avci, M. Gabureac and P. Gambardella: Phys. Rev. Appl. **7** (2017) 014004.
18) D. Weller, W. Reim, K. Spörl and H. Brändle: J. Magn. Magn. Mater. **93** (1991) 183–193.
19) A.P. Mihai, J.P. Attané, A. Marty, P. Warin and Y. Samson: Phys. Rev. B **77** (2008) 060401(R).
20) T.N. Anh Nguyen *et al.*: Sci. Rep. **10** (2020) 10838.
21) W.B. Wu, J. Kasiuk, T.N. Anh Nguyen, J. Fedotova, J. Przewoźnik, C. Kapusta, O. Kupreeva, S. Lazarouk, K.T. Do, T.H. Nguyen, H.K. Vu, D.L. Vu and J. Åkerman: Phys. Chem. Chem. Phys. **22** (2020) 3661.
22) H.B. Vasili, M. Gamino, J. Gàzquez, F. Sánchez, M. Valvidares, P. Gargiani, E. Pellegrin and J. Fontcuberta: ACS Appl. Mater. Interfaces **10** (2018) 12031–12041.
23) Y. Shiomi, T. Ohtani, S. Iguchi, T. Sasaki, Z. Qiu, H. Nakayama, K. Uchida and E. Saitoh: Appl. Phys. Lett. **104** (2014) 242406.
24) A. Kobs, S. Heße, W. Kreuzpaintner, G. Winkler, D. Lott, P. Weinberger, A. Schreyer and H.P. Oepen: Phys. Rev. Lett. **106** (2011) 217207.
25) A. Philippi-Kobs, A. Farhadi, L. Matheis, D. Lott, A. Chuvilin and H.P. Oepen: Phys. Rev. Lett. **123** (2019) 137201.
26) W. Zhang, M.B. Jungfleisch, W. Jiang, Y. Liu, J.E. Pearson, S.G.E. Velthuis and A. Hoffmann: Phys. Rev. B **91** (2015) 115316.
27) Y. Cui, X. Feng, Q. Zhang, H. Zhou, W. Jiang, J. Cao, D. Xue and X. Fan: Phys. Rev. B **103** (2021) 024415.